Journal of Materials Science: Materials in Electronics (2018) 29:20424–20432
https://doi.org/10.1007/s10854-018-0176-9

Optical spectroscopy and electrical analysis of La^{3+}-doped PVA composite films for varistor and optoelectronic applications

H. Elhosiny Ali[1,2] · Yasmin Khairy[2] · H. Algarni[1] · H. I. Elsaeedy[1] · A. M. Alshehri[1] · I. S. Yahia[1,3]

Received: 7 September 2018 / Accepted: 4 October 2018 / Published online: 16 October 2018

Abstract
Poly(vinyl alcohol), PVA, a matrix with 0, 0.185, 0.37, 1.85, 3.7 and 18.5 wt% of lanthanum (III) nitrate were synthesized by the traditional casting method. The order of the crystal structure and the interaction between the mixtures of the investigated materials were analyzed by X-ray and Fourier transform infrared (FT-IR) spectroscopies, while the Scanning Electron Microscopy (SEM), was used to study the surface images of them. Moreover, the optical filtering via UV/Vis/NIR spectroscopy, dielectric constant as well as the D.C. resistivity measurements that arose by the composite films with various wt% of La^{3+} ion were carried out. The structure study of these samples reveals that not only a cluster arises via La^{3+} ion on the SEM surface, but also, the semi-crystalline phases were confirmed by analyzing the pattern of the XRD and FT-IR. However, due to the complex formation of La^{3+} content in PVA matrix, there is an increment in the transitions strength, E_d, and the oscillator wavelength, λ_0 as well as the index of refractions, while the band gap and the average excitation energy, E_s, were decreased. Furthermore, there is a facility of moving charge carriers across the bands that contribute to the small energy gap via La^{3+}-ion contents which clearly noticed in the dielectric and nonlinear *I–V* characteristics. The forward *I–V* measurement of the samples exhibited two distinct regions with different slopes, which is typical as nonlinear behavior for varistor with high applied voltage. Therefore, we can say that our samples have properties make them suitable to use in the applications of optoelectronic and varistor device.

1 Introduction

Poly (vinyl alcohol), PVA, with fillers has been attracting great interest from the side of the scientists and researchers, due to the widespread and various applications in optoelectronics, micro-optics, ophthalmology, sensors, cutoff laser filters, high field or electrostatic discharge electronic protection [1–6]. The functional fillers may be referred to a particle, ions, nanoparticles or metal oxides. The spread of commercial polyvinyl alcohol attributed to the low cost, ability to soluble synthetic in water, chemically stable, non-toxic and biodegradable [7–13]. Moreover, the super-molecules that created inside the PVA polymers causes an energy gap more than 1 eV. However, the creation of these molecules mainly depends on both the hydrogen bond as well as the electronic coordination [14].

It was reported that the optical properties and the electrical conduction of PVA polymeric films depend on both the type and the percentage of doping contents [15]. Also, the lanthanide ions such as Nd, Sm, Gd, and Er can form hydroxo complexes within the polymer because of three fundamental reasons, firstly the weak electrostatic force with the polar groups in the polymer, secondly its relatively large size ions, and the third one its ability to constitute few covalent bonds [16, 17]. The complex formation between PVA and lanthanide ions produce new properties that are useful for various applications as optical signal amplifiers, optical fibers, and lasers.

There is a lot of research work described the functional optical parameters of PVA doped via the Rare Earth Element (REE) [18, 19]. These industrial vitamins salts are one of the most interest lanthanides that have huge applications in

✉ H. Elhosiny Ali
hibrahim@kku.edu.sa; hitham_ph@zu.edu.eg

[1] Advanced Functional Materials & Optoelectronic Laboratory (AFMOL), Department of Physics, Faculty of Science, King Khalid University, P.O. Box 9004, Abha, Saudi Arabia

[2] Physics Department, Faculty of science, Zagazig University, Zagazig 44519, Egypt

[3] Nanoscience laboratory for environmental and biomedical applications (NLEBA), Semiconductor Lab., Physics Department, Faculty of Education, Ain Shams University, Cairo, Egypt

technology as well as modern science [20]. Each of REE has an electronic structure shows the presence of a filled $5S^2$ and $5P^6$ shells around an incomplete 4f shell [21, 22]. Therefore, REEs with a host polymer material induces mixing of states that lead to new transitions which facilitate effective properties. The primary factor for determining the luminescent behavior of the RE- polymer composites is the interactions between RE luminescent species and the matrix of the polymer [23]. The properties of PVA polymeric materials have various changes when they were doped by an RE salt [24, 25].

Not a lot of work focuses on the details of the optical properties of various levels of La^{3+} ions-doped PVA. Most of the researchers investigated the influence of the different temperature and the frequency on the A.C. conductivity and the relaxation of the dielectric for polyvinylidene fluoride, PVDF, and PVA doped with La^{3+} [25, 26]. On the other hand, others studied the optical properties of PVA doping with various REE chlorides i.e. Gd, La, Er and Y [27]. Moreover, Ali et al. focused only on the influence of the La^{3+} concentration on the structure, absorption and the bandgap in PVA [18].

Therefore, in our work, we are aiming to study the influence of a different weight percent of lanthanum nitrate on (1) the crystallinity with various techniques (like XRD, FTIR, and SEM), (2) the optical parameters such as energy gap, refractive index, transitions strength, E_d, and the oscillator wavelength, $\lambda_{0,}$ which are significant for optical devices, (3) the dielectric and nonlinear *I–V* curves for all as-prepared doped and pure PVA samples at ambient temperature.

2 Experimental procedures

2.1 Synthesis of La^{3+}/PVA films

Commercially, PVA, polyvinyl alcohol (4N purity) was used with raw of 0, 0.005, 0.01, 0.05, 0.1 and 0.5 mol% of Lanthanum (III) Nitrate($La(NO_3)_3.6H_2O$), (5N purity), to elaborate the proposed films which are called hereafter PVA:0 wt% La^{3+} (Pure PVA), PVA:0.185 wt% La^{3+}, PVA:0.37 wt% La^{3+}, PVA:1.85 wt% La^{3+}, PVA:3.7 wt% La^{3+} and PVA:18.5 wt% La^{3+}, respectively. The two materials are supplied from Alfa Aesar Karlsruhe, Germany. The equation that used to calculate the weight percentage (wt%) of the La^{3+} in the PVA matrix is:

$$W\ (\%) = \frac{W_{la}\ X\ 100}{W_{PVA} + W_{la}} \tag{1}$$

where w_{La} and w_{PVA} represent the weights of the dopant ($La(NO_3)_3{\cdot}6H_2O$) and PVA, respectively. The traditional casting process was carried out here to form polymeric doped films [25]. Moreover, after agitating the solution of the mixture for 120 s in ultrasonic, the resulting solvent poured into a flat petri dish. Subsequently, the mixture, put in an oven for 4 days at around 40 °C to dry and evaporate completely the solvent to obtain a homogeneous thickness for prepared composite films. All the final resulting samples are flexible, colorless and transparent and the average recording thickness is 0.08 mm.

2.2 Devices and measurements

Shimadzu model XRD-6000 powder diffractometer with a monochromatic Cu-Kα radiation source of wavelength $\lambda = 1.5418$ Å and diffraction angle rate of 0.02 per second in range $5^0 \leq 2\theta \leq 60°$ was used for detecting the phases developed in the La^{3+} doped PVA films by X-ray diffraction (XRD).

Moreover, Thermo Nicolet 6700 FT-IR spectrometer with usually gauge wavenumber range 400–4000 cm^{-1} was used to determine the functional groups inside the PVA pure and with doping of La^{3+} using transmission spectra.

The surface morphology of La^{3+}/PVA films was analyzed by using Field Emission Scanning Electron Microscopy (FE-SEM; model: JSM-6360) in the backscattered electron mode (BSE).

The transmittance, (*T*), and absorbance, (*Abs*) in the range 190–2500 nm, of La^{3+}/PVA films, were monitored via JASCO V-570 spectrophotometer.

A 4200- SCS KEITHLEY semiconductor characterization framework via sinusoidal applied voltage in frequency range starts from 3 kHz to 10 MHz at 23 °C was used for determining the dielectric capacitance and loss of all the as-prepared La^{3+}-doped PVA films. Also, by using this system, the forward non-linear *I–V* curves of the semiconductor materials were tested. For electrical measurements the films are fixed inside a sample holder with two brass electrodes (cupper (Cu)), and the upper one has a diameter of 1 cm.

3 Results and discussions

3.1 The structure analysis of La^{3+}-doped PVA films

The structural properties of PVA:0 wt% La^{3+}, PVA:0.185 wt% La^{3+}, PVA:0.37 wt% La^{3+}, PVA:1.85 wt% La^{3+}, PVA:3.7 wt% La^{3+} and PVA:18.5 wt% La^{3+}films were examined via XRD patterns. The sharp diffraction lines were not observed in Fig. 1, even though; it can be shown for all as-prepared polymeric films, that there is a gradual decrease in the peaks with relatively broad was detected at around 19.59°. Therefore, this attributed to the semi-crystalline nature of all La^{3+}-doped PVA samples that had amorphous and crystalline regions, like the previous works reported for

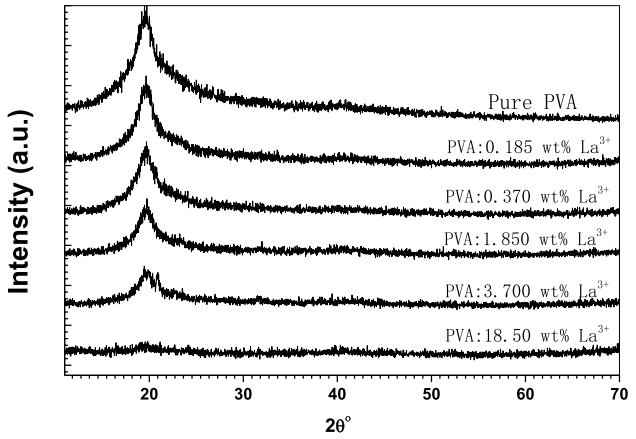

Fig. 1 X-ray diffraction (XRD) pattern of PVA polymer films with various percentages of Lanthanum (III) Nitrate

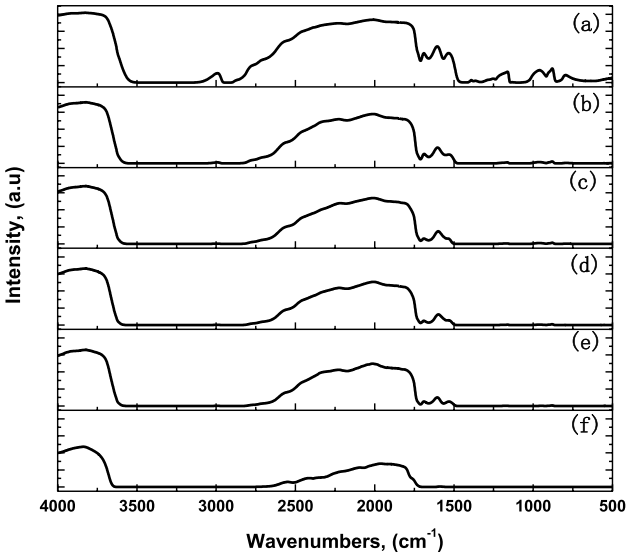

Fig. 2 FTIR spectra of PVA before (*a*) and after doping with 0.185 wt%, (*b*) 0.37 wt% (*c*), 1.85 wt% (*d*), 3.7 wt% (*e*) and 18.5 wt% (*f*) of La^{3+} ions

polymers doped with ions or particles [18, 28]. The reason for these behaviors is the chain interactions of the PVA backbone with La^{3+} ions through the hydrogen bond [29]. So, the reduction of the relative intensity of the characteristic peaks with the increment of lanthanum ion content is due to a strong incorporation in the polymeric samples [30, 31]. Therefore, the crystallinity of the La^{3+}-doped PVA samples was dropped sharply due to the effect of the ions content [32, 33]. This result was similar to that reported for PVA and PVDF doped with lanthanum nitrate/chloride or any other REE ions like Er, Gd, etc., as the crosslinking between the ions and the main group in the polymer, leading to a decrease in the ordering characteristic of the crystalline phase [26, 27, 33].

3.2 The functional groups of La^{3+}-doped PVA films by the analysis of fourier transform infrared (FTIR) spectroscopy

The complex formation at the molecular level associated with the PVA matrix and La^{3+} ion interactions was analyzed. Figure 2a–f showed the FTIR spectra of pure PVA and its complex interactions with various wt% of La^{3+} in the range 500–4000 nm. The main band at 3493–3147 cm^{-1} of O–H stretching vibration in the pure PVA sample were clarified in Fig. 2a. However, the absorption peak at 2942 cm^{-1} is corresponding to asymmetric stretching of CH_2, while the other peaks around 1711 cm^{-1}, 1095 cm^{-1} related to the stretching of C_2 double and CO single bonds. Also, the functional groups of O–H and C–H bending, C–H wagging, as well as C–H vibrations were observed, respectively, at absorption positions 1566 cm^{-1}, 1423 cm^{-1}, 1377 cm^{-1}, and 852 cm^{-1} [34–36].

Moreover, From Fig. 2b–f, the shift of the peaks within La^{3+}-doped PVA films were shown. The strongest characteristic band of the hydroxyl functional group is shifted to 3616–2861 cm^{-1} for PVA:3.7 wt% La^{3+} and PVA: 18.5 wt% La^{3+} films. Also, the intensities of the functional groups were decreased with the more charge accompanied by the increment of lanthanum ion content within a PVA matrix. The shifted peaks indicate the increment of crystalline degradation within the investigated doped PVA polymeric samples due to the strong interaction between the mixtures. As, the broadening in the stretching band of the H-bonds of the polymer main chain during the doping process and therefore, the decrease in the crystalline order is due to the formation of ion-ligand complexes [25, 27]. This result was proved by our XRD experimental and also with that reported in other works [19, 37–39].

3.3 Microstructure surface morphology of La^{3+}-doped PVA films

Figure 3a–f show the morphology surfaces of the PVA:0 wt% La^{3+}, PVA:0.185 wt% La^{3+}, PVA:0.37 wt% La^{3+}, PVA:1.85 wt% La^{3+}, PVA:3.7 wt% La^{3+} and PVA:18.5 wt% La^{3+} by means of scanning electron microscopy (SEM). The morphological surfaces of as-prepared PVA changed by La^{3+} percentages in all films. The black regions are PVA, while whitish spherical dots depict for La^{3+} embedded in the matrix. Although, it was observed that at the concentration of PVA: 0.185 wt% La^{3+}, the particles were well distributed homogeneously over the entire surface, whereas, the high content of La^{3+}, the agglomeration and a cluster of the particles was clearly formed as shown in Fig. 3d–f. The average particle size of

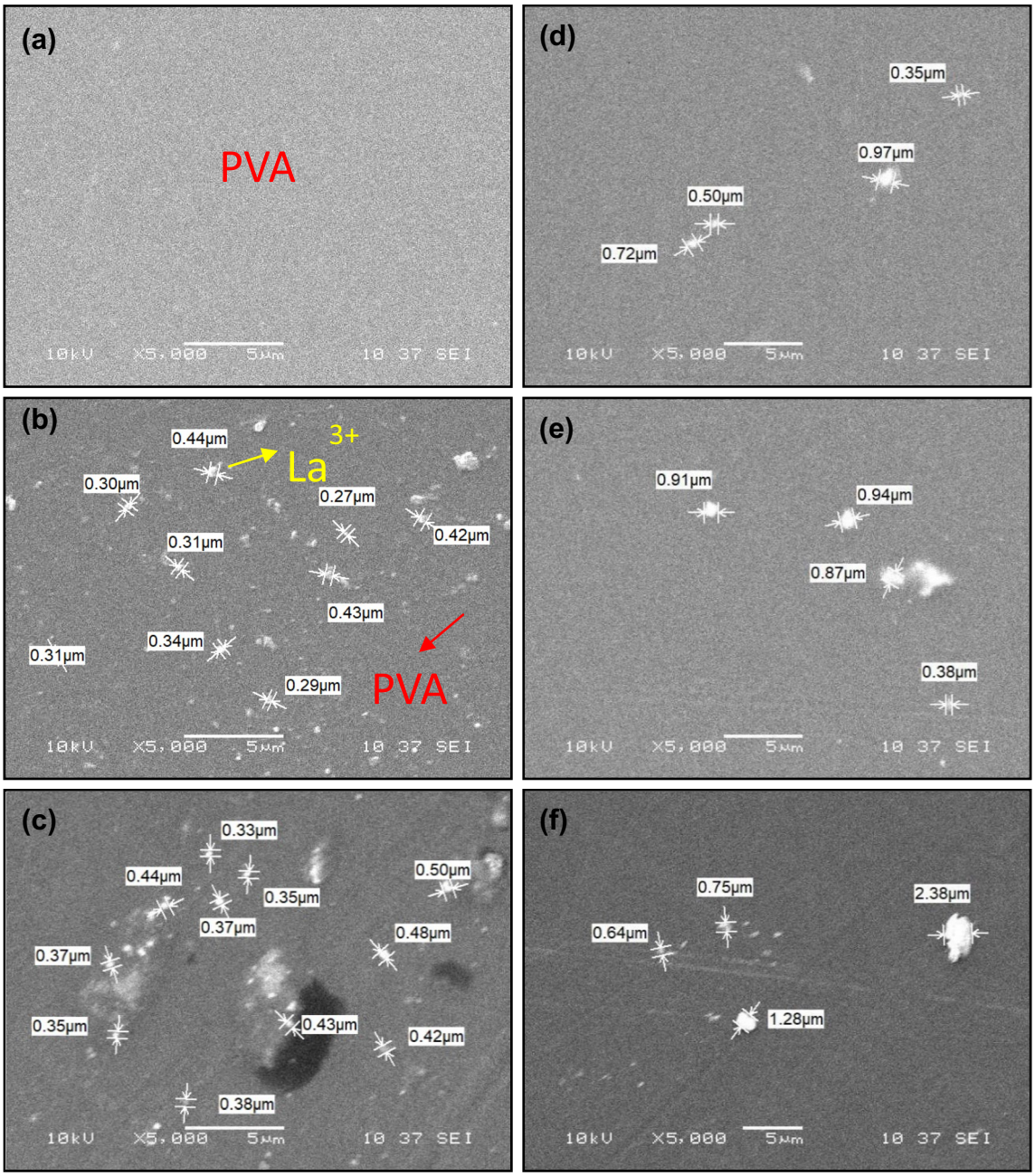

Fig. 3 SEM images of La^{3+}/PVA polymeric composite films of 0 wt% (**a**), 0.185 wt%, (**b**) 0.37 wt% (**c**), 1.85 wt% (**d**), 3.7 wt% (**e**) and 18.5 wt% (**f**) La^{3+} ions

the La^{3+} ion increase with increasing the La^{3+} percentage in the PVA matrix from 0.35 μm for PVA:0.185 wt% La^{3+} to 1.26 μm for PVA:18.5 wt% La^{3+} film which may be due to the formation of ion-ligand complexes at high concentration as well as to minimize the surface energy. This is as the SEM images previously observed in PVA-Al_2O_3, polyvinyl chloride (PVC)/Cadmium oxide, and PVA/graphene oxide nano-composites thin films [40–42].

3.4 The optical analysis of La^{3+}/PVA composite

The optical UV and Vis–NIR transmission spectra were carried out in the region between 190 and 2500 nm for La^{3+}-doped PVA samples. As observed in the Fig. 4, the behavior of the spectra is controlled by the microstructure, which depends on the amount of La^{3+}-contents and their distribution in the polymer matrix. The highest transmitting value that measured in

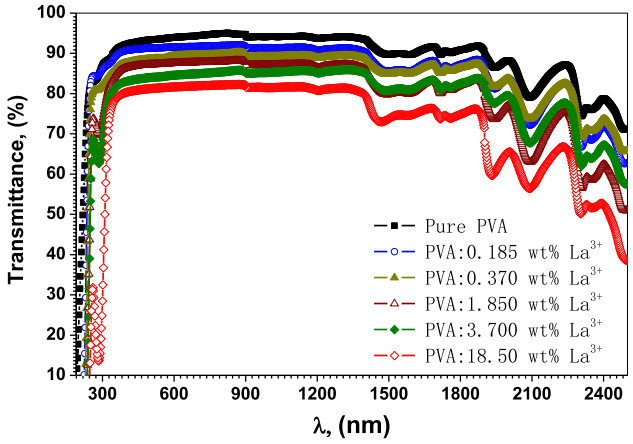

Fig. 4 UV-Vis-NIR transmittance spectra of PVA with different concentration of La^{3+}

the Visible region, was about 93% for pure PVA and gradually decrease to approximately 81% with increasing the La^{3+} ion concentration. These manners were observed previously in several reports of doping PVA polymeric material with RE ions [24], which can be discussed in terms of the disorders within the polymeric samples due to the complexes between ions and cations via O–H groups [43]. In Fig. 5, the peak of the optical absorption at approximately 283 nm of the La^{3+}/PVA polymeric samples was increased with the content of La^{3+}-ions, a similar vision was demonstrated for Gd^{3+}, Eu^{+3}, Sm^{3+}, and Ce^{3+} in PVA polymeric films [44, 45]. This absorption peak may be assigned to π–π* electronic transition [46]. Therefore, the transmission and absorbance spectroscopy of the as-prepared films depend on the content percentage of the La^{3+} doped in PVA. The typical equation used for the calculation of the absorption coefficients (α) is given by Lambert's law [47]:

$$\alpha = 2.303\frac{B}{X(\mathrm{cm})}, \tag{2}$$

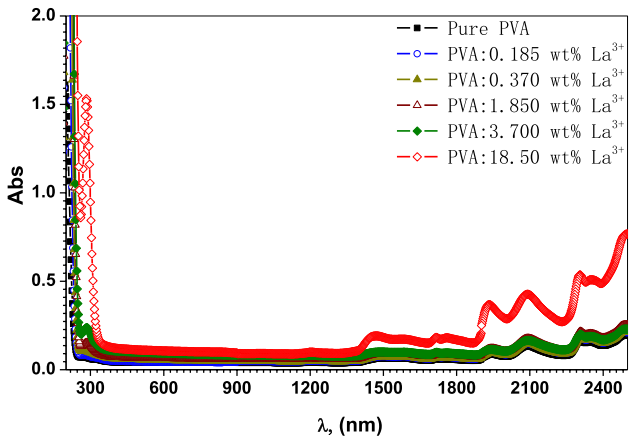

Fig. 5 Absorbance spectra of La^{3+}/PVA polymeric composite films

where B and X represent the absorbance and the thickness in (cm) of the as-prepared films. Figure 6 shows that the absorption coefficients function in the energy ($h\upsilon$) of the photon for PVA with zero (pure) and a different weight percentage of La^{3+}. As was observed, there is a strong dependence absorption coefficient on the La^{3+}-ions content in the studied films. A similar behaviour polymer absorption coefficient on the doping ions was reported in other studies [18, 48]. Also, due to the complex formation in the samples, the absorption edges slightly shifted from 5.34 eV for PVA:0 wt% La^{3+} to low value of 4.72 eV for PVA:18.5 wt% La^{3+} film. This is closer to the value of 20 wt% of La^{3+}-doped PVA that calculated by Ali et al, as the absorption energy = 5.59 eV [18].

A further study on the spectra of the absorbance has been made for determining the optical energy gap and other parameters [49, 50]. The optical band gap E_g^{opt}, of the non-crystalline samples was calculated from Tauc relationship [51]:

$$(\alpha\hbar\omega)^{1/m} = B\left(\hbar\omega - \mathrm{E_g^{opt}}\right), \tag{3}$$

where m can be equal ½ or 2 for, respectively, direct (E_{d1}) and indirect (E_{id1}) transition. As, the values of these allowed transitions were determined by extrapolating the linear portion, of the relation between $(\alpha h\upsilon)^{1/m}$, and ($h\upsilon$), to zero absorption as in Figs. (7, 8). The results that made by Ali et al., and present work have been recorded in Table 1 which shows that the E_{d1}value have been decreased to 4.71 eV for PVA:18.5 wt% La^{3+}, whereas E_{id1} was felled to 4.55 eV for PVA:20 wt% La^{3+} films. This confirmed the decreasing of the band gap with La^{3+}-ion contents [18]. However, these also prove the existence of energy levels that were created in the mobility band gap of the La^{3+}/PVA and so, facilitated the crossing of electrons.

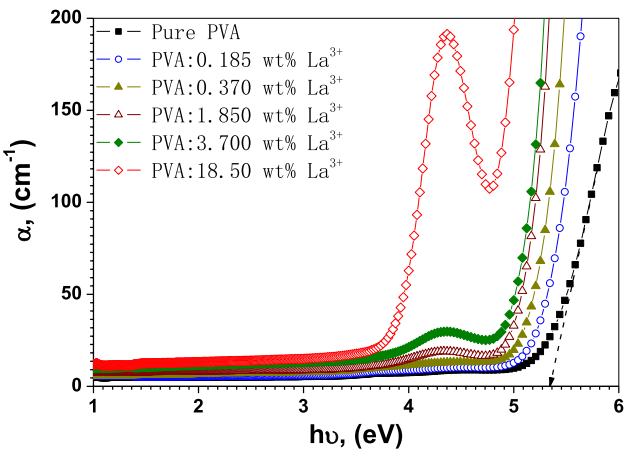

Fig. 6 The absorption coefficient α(hυ) for La^{3+}/PVA polymeric composite films

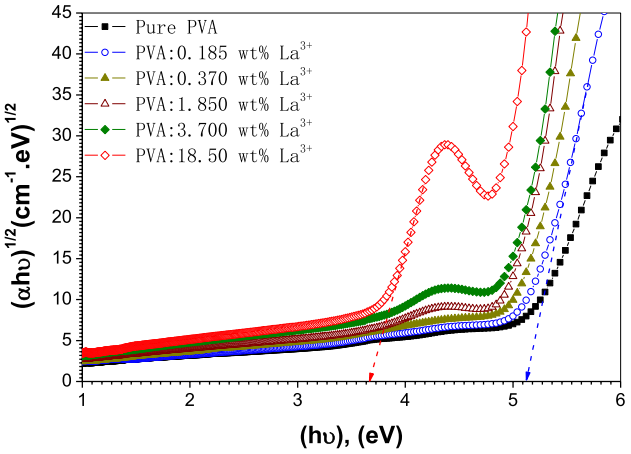

Fig. 7 The variation of $((\alpha h\upsilon))^{1/2}$ as a function of the photon energy for pure different La^{3+}/PVA polymeric composite films

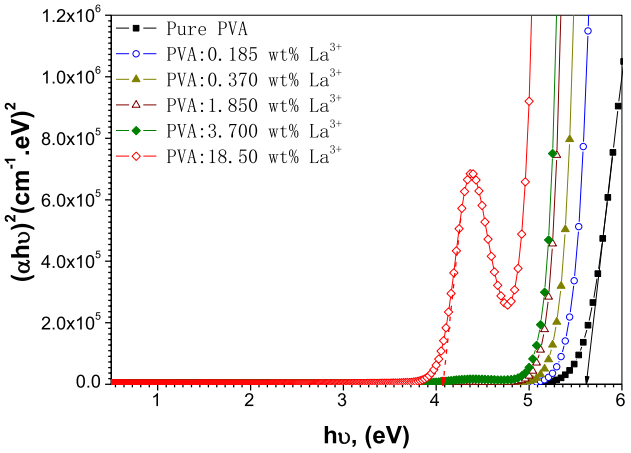

Fig. 8 The variation of $((\alpha h\upsilon))^2$ as a function of the photon energy for different La^{3+}/PVA polymeric composite films

This result shows the engineering band gap of the polymer via the complex interaction between La^{3+} molecules and PVA chains which clearly proved by the results that obtained from the pattern of both XRD and FTIR. The tuning of the band gap leads to La^{3+}-doped PVA samples are suitable for optoelectronic applications [52]. The decreasing of energy gap with the increment of doping was also observed in various works [18, 53, 54].

In order to determine how much the light speed can be reduced in the samples, it is significant to measure the refractive index, n, of all investigated films. Also, n value is an important parameter for optical communication and spectral dispersion devices [55]. Figure 9 shows the variation of n, for pure and La^{3+} doped PVA samples, with the various sets of wavelength values. It was clear from the figure that with increasing the La^{3+} content, the n values of the investigated samples increased which may be due to the interatomic reduction and the changes in the internal structure [19, 27, 41]. Also, it can be seen that the dispersion behavior was decreased, for all pure and La^{3+}-doped PVA samples, at the far wavelength. The maximum value of $n = 2.46$ was obtained by PVA/18.5 wt% La^{3+} film. This value is higher than PVA doped with Er^{3+}ions or PbO_2 [27, 54]. Therefore, it can be used La^{3+}-doped PVA films as antireflection coating materials for solar cells to lenses with high n parameter.

Moreover, for electronic transitions, the energy strength of the inter-band E_d, and the average excitation energy, E_s, in the La^{3+}/PVA samples have been calculated by plotting $1/(n^2-1)$ as a function of $(h\upsilon)^2$ by using the model of the single effective oscillator [56]:

$$\frac{1}{n^2-1} = \frac{E_s}{E_d} - \frac{(h)^2}{E_d E_s}, \tag{4}$$

where n $(h\upsilon)^2$ is the variable refractive index of the present samples. Therefore, the slope of the linear part and the intercept values with the y-axis of that relation used to determine E_d and E_s for all samples (Fig. 10). As observed in Table 1, E_d was increased with La^{+3}-ion contents inside the PVA matrix, while the E_s was decreased. It is noticed that the E_s is closer to E_g. This explains that

Table 1 Direct, indirect energy band gaps and the optical parameters for La^{3+}/PVA polymeric composite films

Composition	E_{d1} (eV)	E_{d2} (eV)	E_{id1} (eV)	E_{id2} (eV)	n	E_d (eV)	E_s (eV)	S_o (10^{-6} nm^{-2})	λ_o (nm)	n_∞
Pue PVA	5.60	–	5.16	–	1.57	7.02	5.15	30.6	221	1.59
PVA + 0.185 wt% La^{3+}	5.48	–	5.14	–	1.65	7.58	5.14	29.3	231	1.60
PVA + 0.370 wt% La^{3+}	5.31	–	5.09	–	1.81	8.80	5.06	34.1	233	1.69
PVA + 1.850 wt% La^{3+}	5.19	–	4.96	–	1.86	10.32	4.96	37.4	241	1.79
PVA + 3.700 wt% La^{3+}	5.13	–	4.88	–	2.09	12.44	4.89	47.4	244	1.95
PVA + 18.50 wt% La^{3+}	4.89	4.07	4.56	3.65	2.46	15.93	4.69	64.0	245	2.20
PVA + 4.000 wt% La^{3+} [18]	–	–	4.74	–	–	–	–	–	–	–
PVA + 12.00 wt% La^{3+} [18]	–	–	4.71	–	–	–	–	–	–	–
PVA + 20.00 wt% La^{3+} [18]	–	–	4.55	–	–	–	–	–	–	–

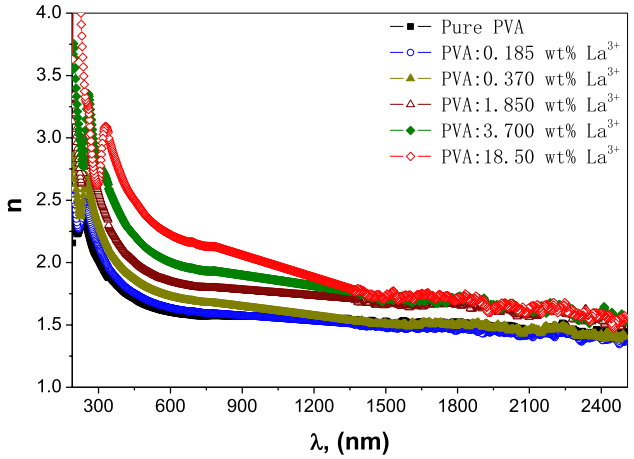

Fig. 9 The refractive index $n\ (\lambda)$ for different concentration of La^{3+}/PVA polymeric composite films

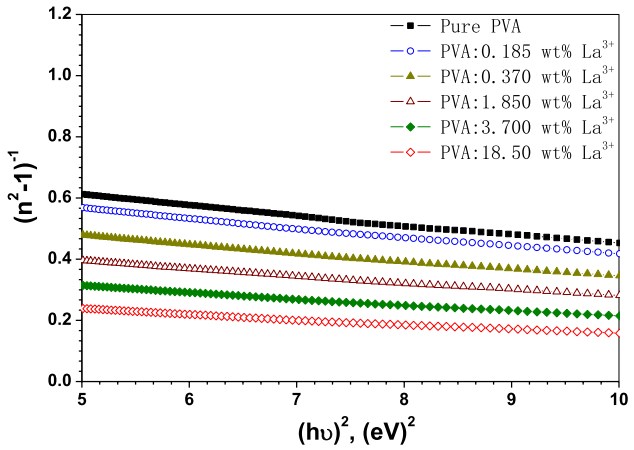

Fig. 10 Variation of $(n^2-1)^{-1}$ with $(h)^2$ for La^{3+}/PVA polymeric composite films

the investigated samples do not follow the single effective oscillator model. As according to this model (Eq. 4), the E_s is related to E_g and the value of the first is twice the second [57].

Other important optical parameters for optoelectronic applications were recorded in Table 1. As the refractive index at long wavelength, n_∞, the average oscillator of wavelength, λ_o, and strength, S_o, are given by plotting a dispersion relation between $1/(n^2-1)$ as a function of the inverse square of the wavelength λ^{-2}, for different concentration of La^{3+}-ions in PVA films (see Fig. 11).

where

$$(n^2-1)^{-1} = (S_0\ \lambda_0)^{-1} + (S_0\ )^{-1}\lambda^{-2}, \tag{5}$$

$$n_\infty^2 = 1 + S_0\lambda^2, \tag{6}$$

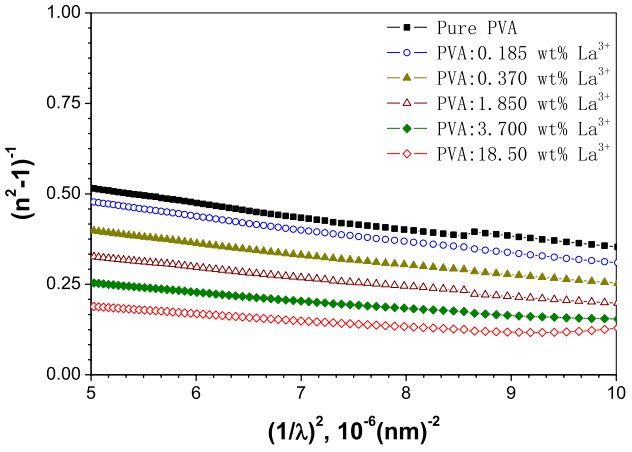

Fig. 11 The dependence of the refractive index $(n^2-1)^{-1}$ on the wavelength $(\lambda)^{-2}$ for La^{3+}/PVA polymeric composite films

The S_0, λ_0 as well as n_∞ are increased with La^{3+}-content in PVA, because of the strong interaction between the two mixtures with increment of doping. Therefore, this suggest that the optical parameters of the present samples can be controlled by La^{3+} percentage and help for their use in opto-applications as well as devices.

3.5 Dielectric measurements of La^{3+}/PVA composite

The formalism of permittivity for the semi-crystalline films gives an important information about the physical and the interaction behavior of the dielectric spectroscopy. It's well known that the main parameter that has an influence on the dielectric properties of the samples is the induced polarization as a function of the external AC field. Moreover, they are largely predictable from the structure of the studied samples [58]. The dielectric constant, ε_1, and the dielectric loss, ε_2, have been calculated using the following simple expressions [59]:

$$\varepsilon_1 = \frac{\mathrm{C\ (F)} \cdot \mathrm{X(m)}}{\varepsilon_0\left(\mathrm{F} \cdot m^{-1}\right) \cdot \mathrm{A}(m^2)}, \tag{7}$$

$$\varepsilon_2 = \varepsilon_1 \cdot \tan\delta, \tag{8}$$

where C is the studied film capacitance. Figure 12a, b represented that ε_1 and d ε_2 values varied with the frequency and the weight percentage of La^{3+}-ions in the PVA backbone [15]. As shown in the Fig. 12a, the ε_1 values were decreased with the weight percentage of La^{3+}-ions, which illustrates the impact of both the complex interaction and the conductivity that cause a decrease of polarization inside the La^{3+}/PVA samples. These results show how much the conducting structural in the La^{3+}-ions will effectively be operating under the different applied frequencies. Moreover, the

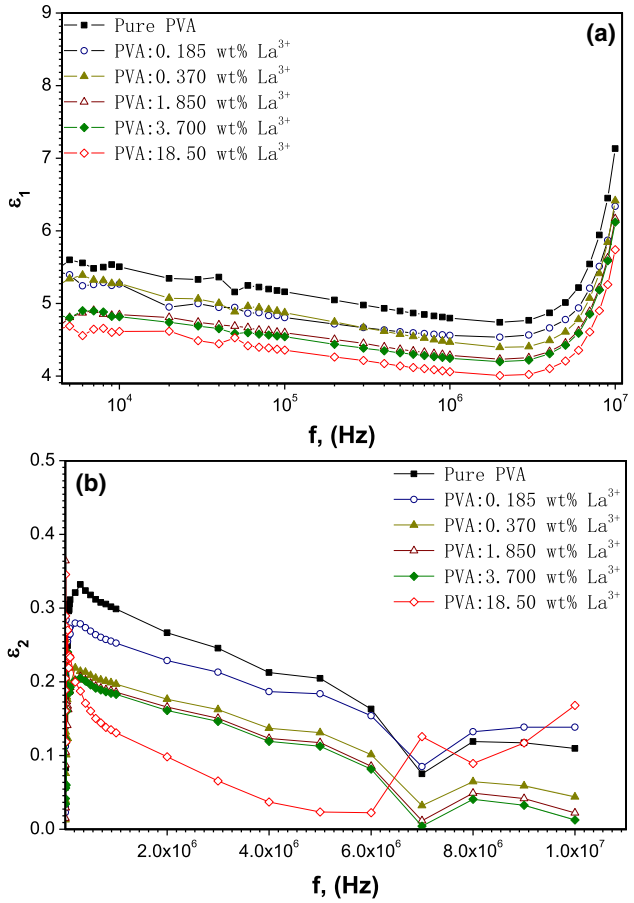

Fig. 12 The dielectric permittivity ε_1 (**a**) and dielectric loss ε_2 (**b**) versus frequency for different La^{3+}/PVA polymeric composite films

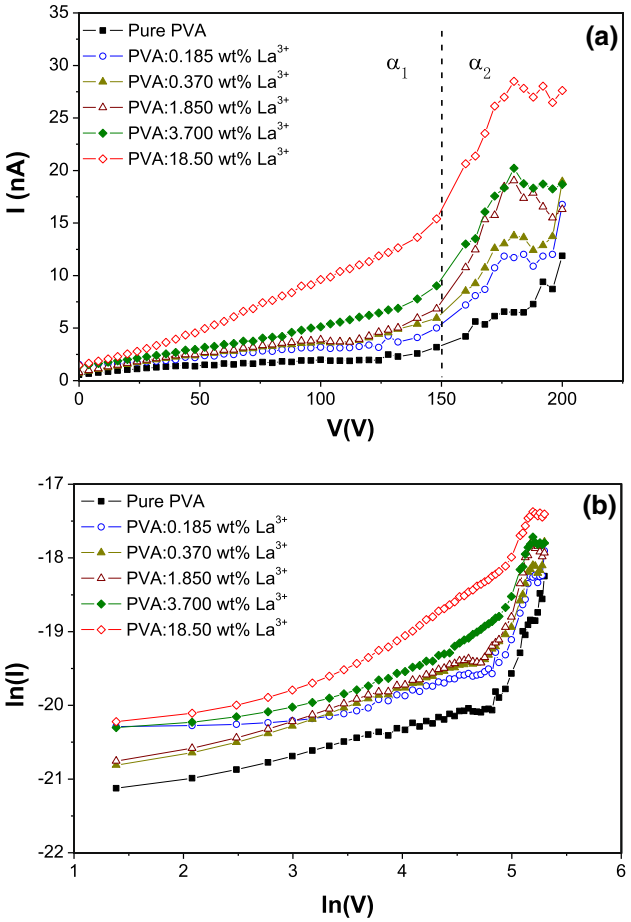

Fig. 13 The *I*–*V* characteristics (**a**) and *ln I*-*ln V* plot (**b**) for various concentration of La^{3+}/PVA polymeric composite films

dielectric loss is higher for PVA:0 wt% La^{3+} film than other doped PVA samples at low frequencies as shown in Fig. 12b, while at high frequencies it increases again. Therefore, this approved that the dielectric loss spectra that associated by molecular motions in the main chain of the La^{3+}/PVA samples were strong frequency influenced. A similar result was found by La^{3+}-doped PVDF films [26].

3.6 *I–V* characteristic curve of La^{3+} doped PVA films

One of the important elements in electronic circuits is the varistor that used as a protection device from excessive baising. It has a nonlinear behavior but different from the diode, as it can work in both directions of current. Figure 13a, b show the *I*–*V* and the corresponding ln*I*-ln*V* nonlinear curves for pure PVA, PVA:0.185 wt% La^{3+}, PVA:0.37 wt% La^{3+}, PVA:1.85 wt% La^{3+}, PVA:3.7 wt% La^{3+} and PVA:18.5 wt% La^{3+} samples. It was observed that there are two regions. The first is linear corresponding to the ohmic resistivity, as the slope (α_1) of the relation between ln*I* and ln*V* is less than 2. This means that the mechanisms of conduction obey Ohm's law controlled due to the entire holes or pinning charge [60]. However, at a high voltage of more than 150V, the nonlinear curve was clearly observed. This illustrated that at high voltage the resistance of the investigated samples was decreased, i.e. the conductance and the current increased. In this nonlinear part, the slope (α_2) is more than 3 which is a characteristic of SCLC (space charge limiting current). The injected carriers of La^{3+} ions are localized via traps in the energy gap, resulting in the formation of space charge against the applied voltage and limits the conduction [61]. This trap was formed by the structural defects that originated during the doping of La^{3+} ions in PVA. These illustrate that characteristic of *I*–*V* curves for La^{3+} doped PVA is typical as varistor devices.

4 Conclusions

This work made a comprehensive survey and deep study on the effect of La^{3+} additions on the microstructure, optical parameters as well as the dielectric of PVA:0 wt% La^{3+},

PVA:0.185 wt% La^{3+}, PVA:0.37 wt% La^{3+}, PVA:1.85 wt% La^{3+}, PVA:3.7 wt% La^{3+} and PVA:18.5 wt% La^{3+} samples. While E_d, λ_o, and n were increased due to the more complex interaction via the O–H groups that arises with the increment of La^{3+} content in PVA matrix, a decrease in the optical band gap, E_g, was associated via this form. Also, the E_s values are closer to E_g. Moreover, the ε_1,and ε_2,were also influenced by La^{3+}-ion contents. The *I–V* plot of all samples shows a nonlinear characteristic with two regions of different slopes. Therefore, the properties of the La^{3+}-ions doped PVA samples could be useful to utilize in different optical and high voltage varistor applications.

Acknowledgements The authors extend their appreciation to the Deanship of Scientific Research at King Khalid University for funding this work through research groups program under Grant No. R.G.P.2/13/39.

References

1. A.H. Salama, M. Dawy, A.M.A. Nada, Polym.-Plast. Tech. Eng. **43**, 1067–1083 (2004)
2. C.-C. Lin, W.S. Lee, C.-C. Sun, W.-H. Whu, Ceram. Int. **34**, 131–136 (2008)
3. S. Yahia, A. Bouzidi, H.Y. Zahran, W. Jilani, S. AlFaify, H. Algarni, H. Guermazi, J. Mol. Struct. **1156**, 492–500 (2018)
4. M. Bin Ahmed, A. Fatehi, A. Zakaria, S. Mahmud, S.A. Mohammmadi, Int. J. Mol. Sci. **13**, 15640–15652 (2012)
5. K. Pal, A.K. Banthia, D.K. Majumdar, AAPS Pharm. Sci. Tech. **8**, 21 (2007)
6. L. Jiang, H.-K. Jun, Y.-S. Hoh, J.-Ok Lim, D.D. Lee, J.S. Huh, Sens. Actuator B **105**, 132–137 (2005)
7. M. Mohsen-Nia, F.S.M. Doulabi, J. Adhes. **87**, 1020–1037 (2011)
8. G.K. Prajapati, P.N. Gupta, Nucl. Instrum. Methods Phys. Res. Sect. B **267**, 3328–3332 (2009)
9. I. Vroman, L. Tighzert, Materials **2**, 307–344 (2009)
10. N. Kulshrestha, B. Chatterjee, P.N. Gupta, Mater. Sci. Eng. B **184**, 49–57 (2014)
11. G. Hirankumar, S. Selvasekarapandian, N. Kuwata, J. Kawamura, T. Hattori, J. Power Source **144**, 262–267 (2005)
12. T. Tunc, Ş Altındal, İ Dökme, H. Uslu, J. Electron. Mater. **40**, 157–164 (2011)
13. M. Tabatabaee, M.A. Sharif, F. Vakili, S. Saheli, J. Rare Earths **27**, 356–361 (2009)
14. K.P. MÖrtl, J.-P. Sutter, S. Golhen, L. Ouahab, O. Kahn, Inorg. Chem. **39**, 1626–1627 (2000)
15. S. El Sayed, T.A. Abdel-Baset, A. Hassen, AIP Adv. **4**, 037114 (2014)
16. J. Fernandes, J. Jaud, J. Dexpert-Ghys, C.B. Cabarrecq. Polyhed **20**, 2385–2391 (2001)
17. S.A. Stepanchikova, R.P. Biteykina, A.A. Sava, Open J. Inorg. Chem. **3**, 42–47 (2013)
18. F.M. Ali, F. Maiz, Physica B **530**, 19–23 (2018)
19. T.A. Hamdalla, T.A. Hanafy, A.E. Bekheet, J. Spect. **204867**, 7 (2015)
20. D. Xue, S. Zuo, H. Ratajczak, Physica B **352**, 99–104 (2004)
21. T.A. Hamdalla, S.S. Nafee, Curr. Appl. Phys. **13**, 981–984 (2013)
22. P. Kenyon, Quant. Electr. **26**, 225–284 (2002)
23. S. Moynihan, R. Van Deun, K. Binnemans, J. Krueger, G. Von Papen, A. Kewell, G. Crean, G. Redmond, Opt. Mater. **29**, 1798–1808 (2007)
24. M. Abdelaziz, Physica B **406**, 1300–1307 (2011)
25. T.A. Hanafy, J. App. Phys. **112**, 034102 (2012)
26. T.A. Hassen, S. Hanafy, Elsayed, A. Himanshu, J. App. Phys. **110**, 114119 (2011)
27. T.A. Hamdalla, T.A. Hanafy, Optik. **127**, 878–882 (2016)
28. S. Sarma, P. Datta, Nanosci Nanotechnol. Lett. **2**, 261–265 (2010)
29. N.-H. Chandrakala, B. Ramaraj, J. Alloys Compd. **586**, 333–342 (2014)
30. M. Hema, S. Selvasekerapandian, A. Sakunthala, D. Arunkumar, H. Nithya, Phys. B **403**, 2740–2747 (2008)
31. J. Malathi, M. Kumaravadivel, G.M. Brahmanandhan, M. Hema, R. Selvasekerapandian, J. Non-Cryst. Solid. **356**, 2277–2281 (2010)
32. E. Sheha, H. Khoder, T.S. Shanap, M.G. El-Shaarawy, M.K. El Mansy, Optics **123**, 1161–1166 (2012)
33. O.G. Abdullah, S.B. Aziz, M.A. Rasheed, Results Phys. **6**, 1103–1108 (2016)
34. P.B. Bhargav, V.M. Mohan, A.K. Sharma, V. Rao, Ion. **13**, 173–178 (2007)
35. N.-H. Chandrakala, B. Ramaraj, G.-M. Madhu, J. Mater. Sci. **47**, 8076–8084 (2012)
36. S.F. Bdewi, O. Abdullah, B.K. Aziz, A. Mutar, J. Inorg. Organomet Polym. **26**, 326–334 (2016)
37. M. Abreha, A.R. Subrahmanyam, J.S. Kumar, Chem. Phys. Lett. **658**, 240–247 (2016)
38. A.R. Polu, H.W. Rhee, J. Ind. Eng. Chem. **37**, 347–353 (2016)
39. P. Pradeepa, G. Sowmya, S. Edwinraj, G.F. Begum, M.R. Prabhu, Mater. Today **3**, 2187–2196 (2016)
40. S. More, R. Dhokne, S. Moharil, Polym. Bull. **75**, 909–923 (2018)
41. A.M. Elsayed, S. Elsayed, W.M. Morsi, S. Mahrous, A. Hassen, Polym. Compd. **35**, 9 (2014)
42. M.N. Muralidharan, S. Mathew, A. Seema, P. Radhakrishnan, Mater. Chem. Phys. **171**, 367–373 (2016)
43. O.G. Abdullah, D.R. Saber, S.A. Taha, Adv. Mater. Lett. **6**, 153–157 (2015)
44. B. Karthikeyan, Chem. Phys. Lett. **432**, 513–517 (2006)
45. K.H. Mahmoud, Z.M. El, A.I. Hanafy, J. Phys. Chem. Solid. **72**, 1057–1065 (2011)
46. A.-M. Albu, I. Maior, C.A. Nicolae, F.L. Bocaneala, Electrochim Acta **211**, 911–917 (2016)
47. K.S. Hemalatha, K. Rukmani, N. Suriyamurthy, B.M. Nagabhushana, Mater. Res. Bull. **51**, 438–446 (2014)
48. S. Asha, Y. Sangappa, S. Ganesh, J. Spectrosc. **879296**, 1–7 (2015)
49. O. Abdullah, D.A. Tahir, K. Kadir, J. Mater. Sci. Mater Electron **26**, 6939–6944 (2015)
50. E.M. Abdelrazek, I.S. Elashmawi, A. El-khodary, A. Yassin, Curr. Appl. Phys. **10**, 607–613 (2010)
51. N.F. Mott, N.F. Davis, Oxford University Press (1979)
52. H.N. Chandrala, B. Ramaraj, M. Shivakumaraiah, G. Siddaramaiah, J. Alloys Compd. **586**, 333–342 (2014)
53. I.S. Yahia, S.M. Keshk, Opt. Laser Technol. **90**, 197–200 (2017)
54. R.T. Abdulwahid, O.G. Abdullah, S.B. Aziz, S.A. Hussein, F.F. Muhammad, M.Y. Yahya, J. Mater. Sci. **27**, 12112–12118 (2016)
55. I. Saini, J. Rozra, N. Chandak, S. Aggarwal, P.K. Sharma, A. Sharma, Mater. Chem. Phys. **139**, 802–810 (2013)
56. N.M. Shah, J.R. Ray, K.J. Patel et al. Thin Solid Film **517**, 3639–3644 (2009)
57. F.F. Muhammad, S.B. Aziz, S.A. Hussein, J. Mater. Sci. Mater. Electron. **26**, 521–529 (2014)
58. A. Karmakar, A. Ghosh, J. Appl. Phys. **110**, 134101 (2011)
59. A. Tataroglu, S. Altındal, M.M. Bulbul, Microelectron. Eng. **81**, 140–149 (2005)
60. V. Janardhanam, I. Iyothi, J.-H. Lee, J.-Y. Kim, V.R. Reddy, C.-J. Choi, Mater. Trans. **55**, 758–762 (2014)
61. I.S. Yahia, G.B. Sakr, T. Wojtowicz, G. Karczewski, Semicond. Sci. Technol. 25, 095001 (2010)